

# Surface-Wave Images of Western Canada: Lithospheric Variations Across the Cordillera/Craton Boundary

**T. Zaporozan**, Department of Geological Sciences, University of Manitoba,  
oro@myumanitoba.ca

**A.W. Frederiksen<sup>1</sup>**, Department of Geological Sciences, University of Manitoba,  
w.frederiksen@umanitoba.ca

**A. Bryksin**, Department of Geological Sciences, University of Manitoba,  
s@gmail.com

**F. Darbyshire**, Centre de recherche GEOTOP, Université du Québec à Montréal,  
hire.fiona\_ann@uqam.ca

Manuscript for *Canadian Journal of Earth Sciences*, revised for resubmission.

<sup>1</sup> Corresponding author. Full address: A.W. Frederiksen, Department of Geological Sciences, University of Manitoba, 125 Dysart Road, Winnipeg, MB, Canada, R3T 2N2. 204-474-9470

*Zaporozan et al., Surface-Wave Images of Western Canada, draft for resubmission*16    **Abstract**

17              Two-station surface-wave analysis was used to measure Rayleigh-wave phase velocities  
18    between 105 station pairs in western Canada, straddling the boundary between the tectonically  
19    active Cordillera and the adjacent stable craton. Major variations in phase velocity are seen  
20    across the boundary at periods from 15 to 200 s, periods primarily sensitive to upper-mantle  
21    structure. Tomographic inversion of these phase velocities was used to generate phase-velocity  
22    maps at these periods, indicating a sharp contrast between low-velocity Cordilleran upper mantle  
23    and high-velocity cratonic lithosphere. Depth inversion along selected transects indicates that the  
24    Cordillera/craton upper-mantle contact varies in dip along the deformation front, with cratonic  
25    lithosphere of the Talson province overthrusting Cordilleran asthenosphere in the northern  
26    Cordillera, and Cordilleran asthenosphere overthrusting Wopmay lithosphere further south.  
27    Localized high-velocity features at sub-lithospheric depths beneath the Cordillera are interpreted  
28    as Farallon slab fragments, with the gap between these features indicating a slab window. A  
29    high-velocity feature in the lower lithosphere of the Slave province may be related to Proterozoic  
30    or Archean subduction.

31

32    **Keywords:** Seismology, surface waves, tomography, Cordillera, craton

33

34

35 **1. Introduction**

36       The lithosphere beneath stable continental regions typically exhibits elevated seismic  
37    velocities to depths of 200 km or more, which has been attributed to a combination of low  
38    temperature and depleted composition (e.g. King 2005, Artemieva 2009, Aulbach 2012). By  
39    contrast, young orogenic belts are underlain by low-velocity upper mantle, attributed to a  
40    combination of high temperature, elevated volatile content, and a component of partial melt (see  
41    e.g. Hyndman et al. 2009). In North America, these two lithospheric regimes exist in close  
42    juxtaposition where the Phanerozoic Cordilleran Orogen abuts on Precambrian ancestral North  
43    America (Figure 1). Previous tomographic studies of North America (van der Lee and Nolet  
44    1997a, Frederiksen et al. 2001, Bedle and Van der Lee 2009, Schaeffer and Lebedev 2014)  
45    image the Cordillera-craton transition as a major lithospheric velocity contrast, but questions  
46    remain regarding the sharpness of the transition, its orientation in three dimensions, and its  
47    relationship to crustal boundaries. We present a new study of the upper mantle beneath western  
48    Canada, based on two-station surface-wave analysis, that brings new constraints to bear on these  
49    questions.

50       East of the Cordillera, Western Canada is a Precambrian craton assemblage accreted in  
51    the Proterozoic from Archean and younger blocks (Whitmeyer and Karlstrom 2007). The Slave,  
52    Superior, Rae, Hearne, and Sask cratons are all of Archean age. These cratons assembled during  
53    the Proterozoic via the Taltson, Wopmay, and Trans-Hudson orogens. Their western boundary  
54    was a passive rifted margin in the Late Proterozoic (Gabrielse and Yorath 1991), onto which a  
55    series of terranes were accreted, beginning with the Intermontane Superterrane in the Jurassic  
56    (Clowes et al. 2005). This collision produced a fold-and-thrust belt extending to the current

*Zaporozan et al., Surface-Wave Images of Western Canada, draft for resubmission*

57 Cordilleran deformation front. A later collision of the Insular Superterrane in the Cretaceous  
58 extended the Cordillera westward to its present extent.

59 **2. Data and analysis**

60 The Geological Survey of Canada (GSC) operates the Canadian National Seismograph  
61 Network (CNSN), which has been recording digital broadband data since the early 1990s (North  
62 and Basham 1993). Further instrumentation was installed as part of the Portable Observatories  
63 for Lithospheric Analysis and Research Investigating Seismicity (POLARIS) project (Eaton et al.  
64 2005), the data from which is also archived by the GSC. We collected data from CNSN and  
65 POLARIS stations in western and central Canada, corresponding to earthquakes of magnitude  
66 greater than 6, at any distance from the receivers, whose propagation paths lay within  $5^{\circ}$  of the  
67 paths between selected station pairs (Figure 2). These pairs were selected to give consistent  
68 coverage of western Canada, and do not include all possible station pairs, particularly in western  
69 British Columbia where stations are more closely spaced than is appropriate for the intended  
70 resolution of this study. The downloaded data were inspected for Rayleigh-wave signal quality  
71 before use. The station responses were removed by conversion to displacement before further  
72 analysis; all stations used are broad-band, with all but two stations (ILKN and VGZ) having  
73 significant velocity response (at least 10% of the peak value) to periods of 200 s or longer. A plot  
74 of instrument responses is provided as supplemental material.

75 Two-station surface-wave analysis is a widely-used technique with a long history  
76 (beginning with Sato 1955) in which the change in waveform between two receiving stations is  
77 measured. Under the assumption that the waveform change is determined entirely by the  
78 structure along the great-circle path connecting the station pair, the waveform change may be  
79 used to isolate structure between the receiving instruments, even in aseismic regions. Thus, two-

*Zaporozan et al., Surface-Wave Images of Western Canada, draft for resubmission*

80 station analysis is appropriate for Canada, which has limited seismic activity away from the west  
81 coast; previous studies have successfully applied this approach to the Canadian Arctic  
82 (Darbyshire 2005), Hudson Bay (Darbyshire and Eaton 2010), the Superior Province (Darbyshire  
83 et al. 2007), the southern Cordillera (Bao et al. 2014), and the northern Cordillera (McLellan et  
84 al. 2018).

85 Two-station analysis is generally applied at large distances from the earthquake source.  
86 Under these conditions, the different surface-wave modes are well separated and the fundamental  
87 Rayleigh mode dominates vertical-component recordings. A single mode's propagation may be  
88 described by a dispersion curve showing the relationship between frequency and velocity; the  
89 velocity considered may be either group velocity (velocity of energy transport, measured by  
90 determining the travel time of the signal envelope peak) or phase velocity (velocity of the phase  
91 of a single frequency, measured by determining the phase shift over a given distance). As the  
92 group velocity dispersion curve may be determined from the phase velocity, but not vice versa,  
93 the phase velocity contains more information (see e.g. Stein and Wysession 2003).

94 We measure phase-velocity dispersion curves using the cross-correlation technique of  
95 Meier et al. (2004); an example is given in Figure 3. Two vertical-component recordings of the  
96 same event, at stations that lie within  $5^\circ$  of a common great-circle path to the source, are cross-  
97 correlated. The phase of the cross-correlation corresponds to the phase difference between the  
98 two traces, with an ambiguity of  $2\pi n$  radians, where  $n$  is an integer. For a cross-correlation phase  
99 of  $\Phi$  measured between two stations separated by a distance  $x$  at angular frequency  $\omega$ , the phase  
100 velocity will be

$$101 \quad c(\omega) = \frac{x\omega}{\phi + 2\pi n}$$

*Zaporozan et al., Surface-Wave Images of Western Canada, draft for resubmission*

102 and therefore multiple velocities are compatible with the measurement, the possible solutions  
103 being more closely spaced at higher frequencies. In practical use, the distance  $x$  is taken to be the  
104 difference between the source-receiver distances for each station, to avoid biased measurements  
105 for events not perfectly aligned with the two-station path. At sufficiently low frequency, there is  
106 likely to be only one phase-velocity value that falls within a realistic range; thus, the approach of  
107 Meier et al. (2004) is to begin at the longest period with significant coherent energy, and  
108 continue the dispersion curve to higher frequencies while assuming that the curve is smooth (as  
109 large jumps in phase velocity are unphysical). Multiple events were analysed for each station  
110 pair, incorporating paths travelling in both possible directions, and the resulting set of dispersion  
111 curves was averaged to obtain a single high-quality curve for each station pair. Two stages of  
112 quality control were performed: on individual paths, events were included in the average only in  
113 frequency bands that showed consistency with other events, and on the averaged curves, paths  
114 were edited to exclude frequency bands with strong deviations (more than 5%) from the average  
115 of all paths.

116 **3. Results**

117 **3.1 Dispersion curves**

118 Figure 4 shows the complete set of dispersion curves obtained in this study, after quality  
119 control was performed. A total of 105 curves was measured, at periods ranging from 16 to 333 s  
120 depending on path length and data quality; generally speaking, longer periods were measurable  
121 on longer paths and shorter periods on shorter paths. We do not, however, have high confidence  
122 in the longest periods, which are sparsely sampled, and therefore only periods up to 200 s are  
123 shown in the figure. The curves all show a velocity that increases with period, as would be  
124 expected given that longer periods sample greater depths. In the 40-200 second range, which is

*Zaporozan et al., Surface-Wave Images of Western Canada, draft for resubmission*

125 most sensitive to lithospheric depths, the path-to-path variation covers a range of  $\approx 400$  m/s. This  
126 variation is systematic with path location, with eastern paths being faster and western paths being  
127 slower.

128 The spatial variation of phase velocities is more apparent in map view (Figure 5). At  
129 relatively short periods (up to 50 s), low velocities are clearly restricted to the Cordillera, while  
130 moderate to high velocities occur further east. At longer periods, more paths sampling both areas  
131 are present; though there is still a trend of velocity increasing eastward, there are also a number  
132 of crossing paths with distinctly different velocities. The true distribution of phase velocity  
133 cannot be determined without tomographic inversion.

### 134 **3.2 Tomographic resolution and maps**

135 Under the assumption that two-station measurements represent averages along great-  
136 circle paths, the recovery of 2-D dispersion maps is a linear inverse problem (Montagner 1986).  
137 We solved for a grid of phase velocities spaced  $1^\circ$  apart in latitude and  $2^\circ$  in longitude, with  
138 smoothing and damping constraints; the correct regularization level was determined by the L-  
139 curve method (Parker 1994). Each period was solved for independently, yielding maps from 30  
140 to 160 s at 10 s intervals.

141 We performed lateral resolution tests using the path coverage for three relevant periods  
142 (50, 80, and 120 s; Figure 6). For an input model consisting of  $4^\circ$  (latitude) by  $8^\circ$  (longitude)  
143 blocks of alternating positive and negative 0.4 km/s velocity perturbations, we calculated average  
144 velocities for each path, added errors comparable to the scatter in the real data, and inverted  
145 using the same parameters as for the real data. The size of the blocks used reflects the feature  
146 size we are able to recover:  $\sim 450$  km over most of the map area. The results indicate that the  
147 boundaries of features of this scale can be recovered accurately (within  $\sim 100$  km) west of  $\sim$

*Zaporozan et al., Surface-Wave Images of Western Canada, draft for resubmission*

148 100°W and south of 70°N, albeit with significant underestimation of anomaly magnitudes, and  
149 that resolution is best at moderate periods (60-100 s). Given that our regularization is smoothing-  
150 based, larger-scale features than this will be recovered more accurately.

151 Final dispersion maps for the real data set are shown in Figure 7. The Cordillera is low-  
152 velocity at all periods, with the edge of the low-velocity region corresponding closely to the  
153 Cordillera/craton boundary at periods of 80 s and less. At longer periods, the edge is more  
154 complex, with low velocities extending some distance into the craton north of 52°N. The  
155 Cordilleran low-velocity region is truncated north of 65°N at all periods; its southern and  
156 western boundaries are not imaged by this study.

157 East of the Cordillera, phase velocities are moderate to high (e.g. > 4.2 km/s at 80 s  
158 period). At short periods, resolution does not extend much east of 110°W due to a lack of high-  
159 frequency measurements along the longer paths in the eastern portion of the model. At periods of  
160 80 s and higher, the highest phase velocities detected are at the eastern edge of the resolved  
161 region, ca. 95°W. Localized high-velocity zones are detected beneath Great Slave Lake (at the  
162 southern tip of the Slave Province) and along the southern edge of the model ca. 110°W.

### 163 **3.3 Depth inversion and cross-sections**

164 Rayleigh-wave period is often used as a depth proxy in surface-wave studies due to the  
165 increase in depth sensitivity with period; however, as any given velocity measurement is  
166 sensitive to a large range of depths, phase velocities must be inverted in order to constrain  
167 seismic velocity as a function of depth. The depth sensitivity of Rayleigh-wave phase velocities  
168 is model-dependent, requiring a nonlinear depth inversion.

169 We inverted for depth using the widely-used Computer Programs in Seismology package  
170 (Herrmann 2013), using phase velocities extracted from the tomographic maps, at periods

*Zaporozan et al., Surface-Wave Images of Western Canada, draft for resubmission*

171 ranging from 30 to 160 s at 10 s intervals, the range of periods at which we are most confident in  
172 the map coverage. We used a starting model simplified from IASP91 (Kennett and Engdahl  
173 1991), with fixed layer thicknesses ranging from 15 to 25 km (including a two-layer crust 35 km  
174 thick; see Figure 8), and inverted for S velocity over 5 iterations, with P velocity determined  
175 using a Poisson's ratio fixed to match the base model values (which range from 0.20 to 0.29),  
176 and density calculated from the P velocity. Smoothing regularization was used to compensate for  
177 the non-uniqueness of the inversion and to encourage model simplicity.

178 Synthetic tests of the depth inversion are shown in Figure 8. For each test, an input model  
179 containing a large (300 m/s) perturbation from IASP91 was used to generate a dispersion curve,  
180 using the same period sampling as the real data. The dispersion curve was then inverted (using  
181 the same inversion parameters as the real data) to test recovery of the input. We find that low-  
182 velocity features are significantly smeared, but not missed; high-velocity features at relatively  
183 shallow depth (above 150 km) are recovered, but produce a weaker low-velocity artefact below,  
184 while deep high-velocity anomalies are poorly recovered. These effects are a consequence of the  
185 non-linearity of surface-wave depth inversion, and will be less severe for weaker velocity  
186 perturbations.

187 To generate cross-sections, we spatially interpolated phase velocities at 50 km intervals  
188 from all dispersion maps, along five great-circle trajectories (Figure 9). The resulting dispersion  
189 curves were then inverted to form 1-D S velocity models, as described above; the 1-D models  
190 were concatenated to form a 2-D model along each transect. An example of this procedure is  
191 given in Figure 10, in which the series of dispersion curves is presented as a pseudosection (top  
192 panel) and inverted to obtain a velocity model (presented in both relative and absolute velocity  
193 terms). It is worth noting that the lack of short-period sampling in some areas affects the

*Zaporozan et al., Surface-Wave Images of Western Canada, draft for resubmission*

194 inversion; northeast of the 1100 km point along the transect, the shortest periods are not available  
195 (due to longer two-station paths in this region) and the shallowest part of the model is not well  
196 constrained. As a consequence, northeast of 1100 km, velocity anomalies appear weaker due to  
197 upward smearing of structure into the poorly-sampled shallow depth range. We therefore expect  
198 that mantle velocity anomalies will be somewhat underestimated in the more poorly-  
199 instrumented portions of the study area; this effect is most pronounced on the AA-AA' section  
200 shown in Figure 10.

201 Transects were selected to examine the Cordillera-craton transition along three near  
202 boundary-perpendicular sections (AA-AA', BB-BB' and CC-CC'), along-strike variation within  
203 the Cordilleran low-velocity anomaly (DD-DD'), and a high-velocity feature detected near Great  
204 Slave Lake in the dispersion maps (EE-EE'). The Cordillera is underlain by a low-velocity  
205 feature (marked as A on the cross-sections; Figures 11 and 12) averaging 2-4% below IASP91  
206 velocity down to ~250 km depth. The adjacent cratonic lithosphere (B) is underlain by high-  
207 velocity lithosphere (5-8% above IASP91) down to 200-250 km depth; the contact between these  
208 two anomalies is quite sharp (~ 8-10% over 200-300 lateral km at lithospheric depths), lies  
209 directly beneath the crustal contact, and is not vertical. In the northern two cross-sections (CC-  
210 CC' and BB-BB'; Figure 11) the contact dips 10-20° to the northeast, with cratonic lithosphere  
211 overlying asthenospheric material associated with the Cordillera; by contrast, the southernmost  
212 section (AA-AA') shows a dip of ~ 30° in the opposite direction. The depth extent of Cordilleran  
213 low velocities varies somewhat along strike, shallowing to ~ 150 km depth beneath southern  
214 British Columbia (DD-DD'; Figure 12). Our synthetic tests showed that high velocities at  
215 lithospheric depths can produce low-velocity artefacts below; however, the artefacts are

*Zaporozan et al., Surface-Wave Images of Western Canada, draft for resubmission*

216 significantly weaker than the high-velocity anomalies they underlie, which is not the case where  
217 feature A underlies feature B.

218 A localized high-velocity zone (feature C) centred on Great Slave Lake ( $62^{\circ}\text{N}$ ,  $115^{\circ}\text{W}$ ) is  
219 visible on longer-period dispersion maps (Figure 7). The two cross-sections that intersect this  
220 zone (BB-BB' and EE-EE'; Figures 11 and 12) show a high-velocity feature from  $\approx 125\text{-}275$  km,  
221 extending somewhat deeper than is typical for cratonic lithosphere in North America (200-250  
222 km; Eaton et al. 2009, Yuan et al. 2014). Even deeper high-velocity features (labelled D) are  
223 seen in patches beneath the Cordillera and adjacent areas.

224 **4. Discussion**

225 The Cordilleran mantle velocities we have measured are very low – for instance, at 400  
226 km along the BB-BB' transect, the lowest mantle S velocity attained is 4.25 km/s from 155-170  
227 km depth. Though a very low value for this depth (IASP91 reaches 4.51 km/s at 160 km), it is  
228 consistent with the models of Van der Lee and Frederiksen (2005) and Schaeffer and Lebedev  
229 (2014), which have comparable velocities in the same location. Based on the velocity-  
230 temperature calculations of Hyndman et al. (2009), this low velocity would correspond to a  
231 temperature of  $\sim 1200\text{-}1250^{\circ}\text{C}$ , which is in accordance with previous studies, implying  
232 asthenospheric material underlying a weak, thin lithosphere and raising the possibility of small-  
233 scale convection in the Cordilleran upper mantle (Hyndman 2010).

234 Though our measurements of Cordilleran upper-mantle velocity primarily confirm earlier  
235 studies, this study provides novel high-resolution constraints on a significant portion of the  
236 Cordillera/craton boundary. Our cross-sections show that the mantle boundary is not vertical  
237 (Figure 11), with some high-velocity material extending west of the Cordilleran deformation

*Zaporozan et al., Surface-Wave Images of Western Canada, draft for resubmission*

238 front in the crust. This may help to explain why some models place the boundary west of the  
239 front (see e.g. Frederiksen et al. 2001, McLellan et al. 2018).

240 Our most remarkable observation at the Cordillera/craton boundary is the change in dip  
241 direction from northeastern (cratonic material overthrusting Cordilleran asthenosphere) on the  
242 northern and central cross-sections (CC-CC' and BB-BB', Figure 11) to southwestern  
243 (Cordilleran asthenosphere overthrusting cratonic lithosphere) in the southernmost cross-section.  
244 This change, which was also detected in a recent North American model (Schaeffer et al. 2017),  
245 is seen in previous smaller-scale models. Surface and body-wave models of the southern  
246 Cordillera (Bao et al. 2014, Chen et al. 2017) show a steeply westward-dipping or vertical  
247 boundary, while models of the northern Cordillera show northeast dips (Cook and Erdmer 2005,  
248 Mercier et al. 2009). Models of the United States are not directly comparable due to the  
249 influence of the Yellowstone hotspot.

250 A possible explanation for the difference in dip direction at the lithospheric contact may  
251 be that the northern two cross-sections sample the Wopmay orogen, while the southernmost  
252 cross-section intersects the Taltson. Though both of these orogens were assembled through  
253 eastward-dipping subduction (McDonough et al. 2000, Davis et al. 2015), their western edges  
254 consist of different terranes (the Hottah for the Wopmay and the Buffalo Head for the Taltson).  
255 These terranes have different origins, and it is possible that their associated lithospheres are  
256 rheologically distinct. Edge-driven convection has been proposed for the southern Cordillera  
257 (Hardebol et al. 2012, Bao et al. 2014); modelling results indicate that mantle viscosity is an  
258 important control on the behaviour of the Cordillera/craton transition. It is thus plausible that a  
259 rheological difference between cratonic lithosphere of different affinity is affecting the shape of  
260 the mantle boundary, but further modelling is needed to support this.

*Zaporozan et al., Surface-Wave Images of Western Canada, draft for resubmission*

261           Localized high-velocity features at sub-lithospheric depths (feature D; Figures 11 and 12)  
262    are found at various points beneath the Cordillera and craton. High velocities at these and greater  
263    depths appear in a number of tomographic models (see e.g. van der Lee and Nolet 1997b, Ren et  
264    al. 2007) and are commonly attributed to remnants of the subducted Farallon or Kula slab. The  
265    lateral resolution of our model does not permit an interpretation of the lateral extent of these  
266    features east of the Cordillera (as shown by the longest-period resolution test in Figure 6).  
267    However, as our path density is highest within the Cordillera itself, the discontinuous nature of  
268    feature D in section DD-DD' is probably a real feature, though ~ 350 km depth is at the limit of  
269    resolution for fundamental-mode Rayleigh waves.

270           Gaps in subducting slabs, resulting from processes such as ridge/trench contact, are  
271    known in the literature as slab windows. Slab windows have been proposed to exist north and  
272    south of the Juan de Fuca slab (Thorkelson and Taylor 1989); the southern window is seen in  
273    northern California (Hawley et al., 2016), while an additional slab gap is visible as a low-  
274    velocity feature beneath Oregon (Tian and Zhao 2012). We interpret feature D as slab remnants  
275    interrupted by a northern Cordilleran slab window, and therefore that the slab is absent from 400-  
276    1200 km along the DD-DD' cross-section. This range corresponds well with lateral velocity  
277    contrasts at  $\approx 50^{\circ}\text{N}$  and  $60^{\circ}\text{N}$  seen in the teleseismic P velocity model of Mercier et al. (2009).

278           The high-velocity feature labelled C in sections BB-BB' and EE-EE' cannot be attributed  
279    to recent subduction. Its depth of 150-250 km beneath the stable craton places it at the base of  
280    the lithosphere; its velocity of up to 10% over IASP91 is remarkable, indicating that it is fast  
281    even relative to the generally high-velocity surrounding cratonic lithosphere. A high-velocity  
282    feature beneath the Slave craton was previously found in this depth range using array analysis of  
283    surface waves (Chen et al. 2007), while strongly-layered lithosphere is visible in receiver

*Zaporozan et al., Surface-Wave Images of Western Canada, draft for resubmission*

284 functions (Bostock 1998). LITHOPROBE reflection data across the Slave craton's eastern boundary  
285 show dipping reflectors attributed to Proterozoic and Archean subduction (Cook et al. 1999)  
286 which, when extrapolated eastward, correspond with receiver-function arrivals bracketing the  
287 depth of feature C. We therefore propose that feature C preserves these subduction remnants in  
288 the lower portion of the Slave lithosphere.

289 **5. Conclusions**

290 Through two-station analysis of surface-wave records, we have mapped Rayleigh phase  
291 velocity across western Canada. The most salient feature of our dispersion maps is the sharp  
292 contrast between low-velocity Cordilleran upper mantle and high-velocity cratonic lithosphere.  
293 By extracting dispersion curves from the tomographic maps and inverting for S velocity  
294 structure, we have generated cross-sections examining the Cordillera/craton mantle boundary  
295 and surrounding region; these cross-sections show a change in dip of the mantle contact from  
296 northeast in the northern Cordillera to southwest in the southern Cordillera, which may reflect  
297 differences in rheology between the Wopmay and Taltson shield provinces. Isolated high-  
298 velocity features seen beneath the Cordilleran upper mantle may represent Farallon slab  
299 fragments, separated by a gap resulting from a Cordilleran slab window. A high-velocity feature  
300 at the base of the Slave Province lithosphere correlates with a previously interpreted Proterozoic  
301 subduction feature.

302 The main limitation on these results is the lack of resolution east of the Cordillera due to  
303 a limited station network. New instruments currently deployed in the Northern Cordillera (Ma  
304 and Audet 2017) will allow improvement of these images in the future, as will incorporation of  
305 instrumentation in the United States.

*Zaporozan et al., Surface-Wave Images of Western Canada, draft for resubmission*306 **Acknowledgements**

307 Funding for this research was provided by NSERC, the Geological Survey of Canada,  
308 and de Beers Canada. Pascal Audet and Ian Ferguson provided essential feedback on the M.Sc.  
309 thesis from which this paper is derived; thanks also to Andrew Schaeffer for helpful discussion.  
310 Thanks to Derek Schutt and an anonymous reviewer for reviews that significantly improved this  
311 manuscript.

312

313 **References**

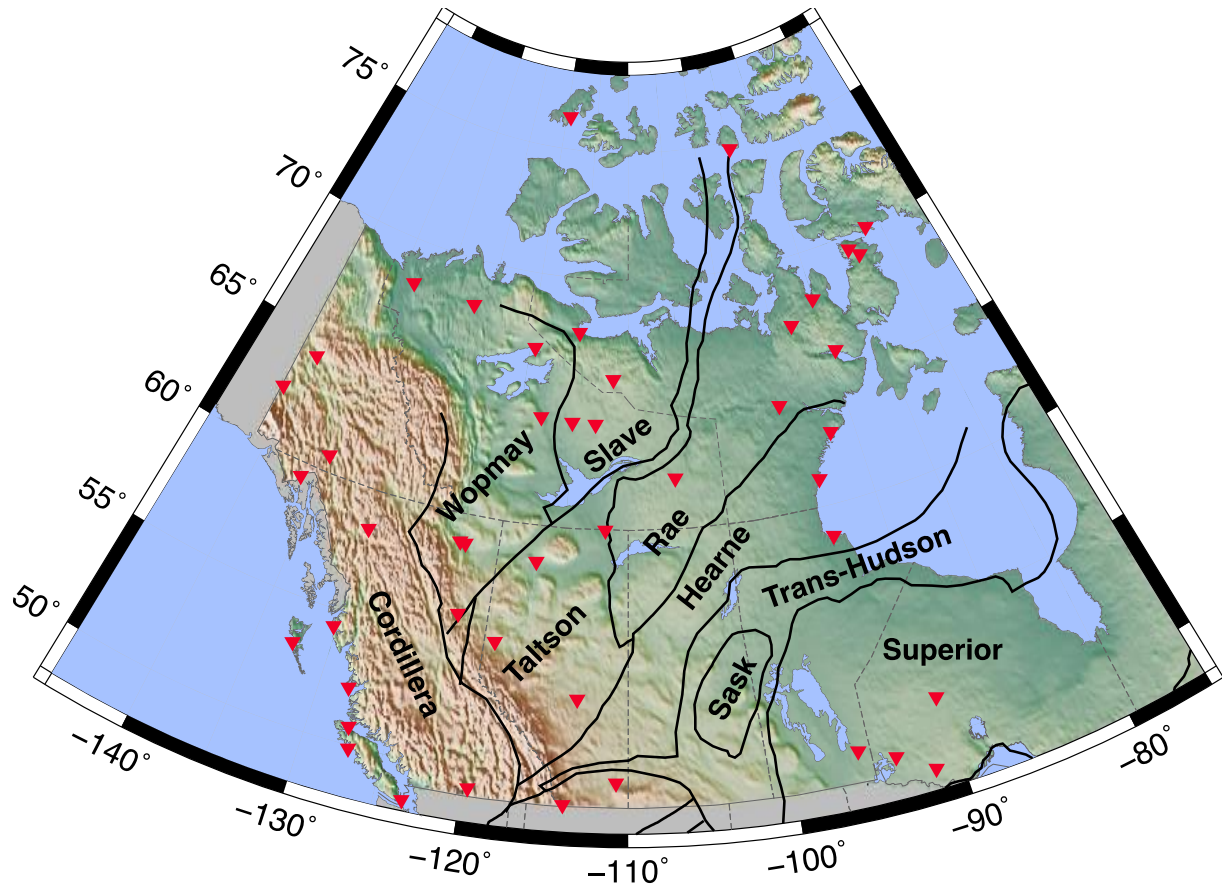
- 314 Artemieva, I.M. 2009. The continental lithosphere: Reconciling thermal, seismic, and petrologic  
 315 data. *Lithos* **109**(1-2): 23–46. doi:10.1016/j.lithos.2008.09.015.
- 316 Aulbach, S. 2012. Craton nucleation and formation of thick lithospheric roots. *Lithos* **149**(C):  
 317 16–30. Elsevier B.V. doi:10.1016/j.lithos.2012.02.011.
- 318 Bao, X., Eaton, D.W., and Guest, B. 2014. Plateau uplift in western Canada caused by  
 319 lithospheric delamination along a craton edge. *Nature Geoscience* **7**(11): 830–833.  
 320 doi:10.1038/ngeo2270.
- 321 Bedle, H., and Van Der Lee, S. 2009. S velocity variations beneath North America. *J Geophys  
 322 Res-Sol Ea* **114**: –. doi:10.1029/2008JB005949.
- 323 Bostock, M.G. 1998. Mantle stratigraphy and evolution of the Slave province. *J. Geophys. Res*  
 324 **103**: 21183–21200.
- 325 Chen, C.-W., Rondenay, S., Weeraratne, D.S., and Snyder, D.B. 2007. New constraints on the  
 326 upper mantle structure of the Slave craton from Rayleigh wave inversion. *Geophys Res Lett*  
 327 **34**: –. doi:10.1029/2007GL029535.
- 328 Chen, Y., Gu, Y.J., and Hung, S.-H. 2017. Finite-frequency P-wave tomography of the Western  
 329 Canada Sedimentary Basin: Implications for the lithospheric evolution in Western Laurentia.  
 330 *Tectonophysics* **698**(C): 79–90. Elsevier B.V. doi:10.1016/j.tecto.2017.01.006.
- 331 Clowes, R., Hammer, P.T., Fernández-Viejo, G., and Welford, J. 2005. Lithospheric structure in  
 332 northwestern Canada from Lithoprobe seismic refraction and related studies: a synthesis.  
 333 *Can J Earth Sci* **42**(6): 1277–1294.
- 334 Cook, F.A., and Erdmer, P. 2005. An 1800 km cross section of the lithosphere through the  
 335 northwestern North American plate: lessons from 4.0 billion years of Earth's history. *Can J  
 336 Earth Sci* **42**: 1295–1311. doi:10.1139/e04-106.
- 337 Cook, F.A., Velden, A.J., Hall, K.W., and Roberts, B.J. 1999. Frozen subduction in Canada's  
 338 Northwest Territories: Lithoprobe deep lithospheric reflection profiling of the western  
 339 Canadian Shield. *Tectonics* **18**(1): 1–24. doi:10.1029/1998TC900016.
- 340 Darbyshire, F.A. 2005. Upper mantle structure of Arctic Canada from Rayleigh wave dispersion.  
 341 *Tectonophysics* **405**(1-4): 1–23. doi:10.1016/j.tecto.2005.02.013.
- 342 Darbyshire, F.A., and Eaton, D.W. 2010. The lithospheric root beneath Hudson Bay, Canada  
 343 from Rayleigh wave dispersion No clear seismological distinction between Archean and  
 344 Proterozoic mantle. *Lithos* **120**: 144–159. doi:10.1016/j.lithos.2010.04.010.
- 345 Darbyshire, F.A., Eaton, D.W., Frederiksen, A., and Ertolahti, L. 2007. New insights into the  
 346 lithosphere beneath the Superior Province from Rayleigh wave dispersion and receiver  
 347 function analysis. *Geophys J Int* **169**: 1043–1068. doi:10.1111/j.1365-246X.2006.03259.x.
- 348 Davis, W.J., Ootes, L., Newton, L., Jackson, V., and Stern, R.A. 2015. Characterization of the  
 349 Paleoproterozoic Hottah terrane, Wopmay Orogen using multi-isotopic (U-Pb, Hf and O)  
 350 detrital zircon analyses: An evaluation of linkages to northwest Laurentian Paleoproterozoic  
 351 domains. *Precambrian Research* **269**: 296–310. Elsevier B.V.  
 352 doi:10.1016/j.precamres.2015.08.012.
- 353 Eaton, D.W., Adams, J., Asudeh, I., Atkinson, G.M., Bostock, M.G., Cassidy, J.F., Ferguson,  
 354 I.J., Samson, C., Snyder, D.B., Tiampo, K.F., and Unsworth, M.J. 2005. Investigating  
 355 Canada's lithosphere and earthquake hazards with portable arrays. *Eos* **86**(17): 169–171.  
 356 doi:10.1029/2005EO170001/full.
- 357 Eaton, D.W., Darbyshire, F.A., Evans, R.L., Grütter, H., Jones, A.G., and Yuan, X. 2009. The

Zaporozan *et al.*, Surface-Wave Images of Western Canada, draft for resubmission

- 358 elusive lithosphere–asthenosphere boundary (LAB) beneath cratons. *Lithos* **109**(1-2): 1–22.  
359 doi:10.1016/j.lithos.2008.05.009.
- 360 Frederiksen, A., Bostock, M.G., and Cassidy, J.F. 2001. S-wave velocity structure of the  
361 Canadian upper mantle. **124**: 175–191.
- 362 Gabrielse, H., and Yorath, C.J. 1991. Tectonic Synthesis. In *Geology of the Cordilleran Orogen*  
363 in Canada. Edited by H. Gabrielse and C.J. Yorath. Accents Publications Service. pp. 677–  
364 705.
- 365 Hardebol, N.J., Pysklywec, R.N., and Stephenson, R. 2012. Small-scale convection at a  
366 continental back-arc to craton transition: Application to the southern Canadian Cordillera.  
367 *Journal of Geophysical Research: Solid Earth* (1978–2012) **117**(B1).  
368 doi:10.1029/2011JB008431.
- 369 Hawley, W.B., Allen, R.M., and Richards, M.A. 2016. Tomography reveals buoyant  
370 asthenosphere accumulating beneath the Juan de Fuca plate. *Science* **353**(6306): 1406–1408.  
371 American Association for the Advancement of Science. doi:10.1126/science.aad8104.
- 372 Herrmann, R.B. 2013. Computer Programs in Seismology: An Evolving Tool for Instruction and  
373 Research. *Seismological Research Letters* **84**(6): 1081–1088. GeoScienceWorld.  
374 doi:10.1785/0220110096.
- 375 Hyndman, R. 2010. The consequences of Canadian Cordillera thermal regime in recent tectonics  
376 and elevation: a review. *Can J Earth Sci* **47**(5): 621–632.
- 377 Hyndman, R.D., Currie, C.A., Mazzotti, S., and Frederiksen, A. 2009. Temperature control of  
378 continental lithosphere elastic thickness, Te vs Vs. *Earth and Planetary Science Letters* **277**:  
379 539–548. doi:10.1016/j.epsl.2008.11.023.
- 380 Kennett, B.L.N., and Engdahl, E.R. 1991. traveltimes for global earthquake location and phase  
381 identification. *Geophysical Journal of the Royal Astronomical Society* **105**(2): 429–465.  
382 Blackwell Publishing Ltd. doi:10.1111/j.1365-246X.1991.tb06724.x.
- 383 King, S.D. 2005. Archean cratons and mantle dynamics. *Earth and Planetary Science Letters*  
384 **234**(1-2): 1–14. doi:10.1016/j.epsl.2005.03.007.
- 385 Ma, S., and Audet, P. 2017. Seismic velocity model of the crust in the northern Canadian  
386 Cordillera from Rayleigh wave dispersion data. **54**(2): 163–172. doi:10.1139/cjes-2016-  
387 0115.
- 388 McDonough, M.R., McNicoll, V.J., Schetselaar, E.M., and Grover, T.W. 2000.  
389 Geochronological and kinematic constraints on crustal shortening and escape in a two-sided  
390 oblique-slip collisional and magmatic orogen, Paleoproterozoic Talson magmatic zone,  
391 northeastern Alberta. *Can J Earth Sci* **37**: 1549–1573.
- 392 McLellan, M., Schaeffer, A.J., and Audet, P. 2018. Structure and fabric of the crust and  
393 uppermost mantle in the northern Canadian Cordillera from Rayleigh-wave tomography.  
394 *Tectonophysics* **724-725**: 28–41. Elsevier. doi:10.1016/j.tecto.2018.01.011.
- 395 Meier, T., Dietrich, K., Stöckhert, B., and Harjes, H.-P. 2004. One-dimensional models of shear  
396 wave velocity for the eastern Mediterranean obtained from the inversion of Rayleigh wave  
397 phase velocities and tectonic implications. *Geophys J Int* **156**(1): 45–58. doi:10.1111/j.1365-  
398 246X.2004.02121.x.
- 399 Mercier, J.P., Bostock, M.G., Cassidy, J.F., Dueker, K., Gaherty, J.B., Garnero, E.J., Revenaugh,  
400 J., and Zandt, G. 2009. Body-wave tomography of western Canada. *Tectonophysics* **475**(3-  
401 4): 480–492. doi:10.1016/j.tecto.2009.05.030.
- 402 Montagner, J.P. 1986. Regional three-dimensional structures using long-period surface waves.  
403 *Ann Geophys.*

*Zaporozan et al., Surface-Wave Images of Western Canada, draft for resubmission*

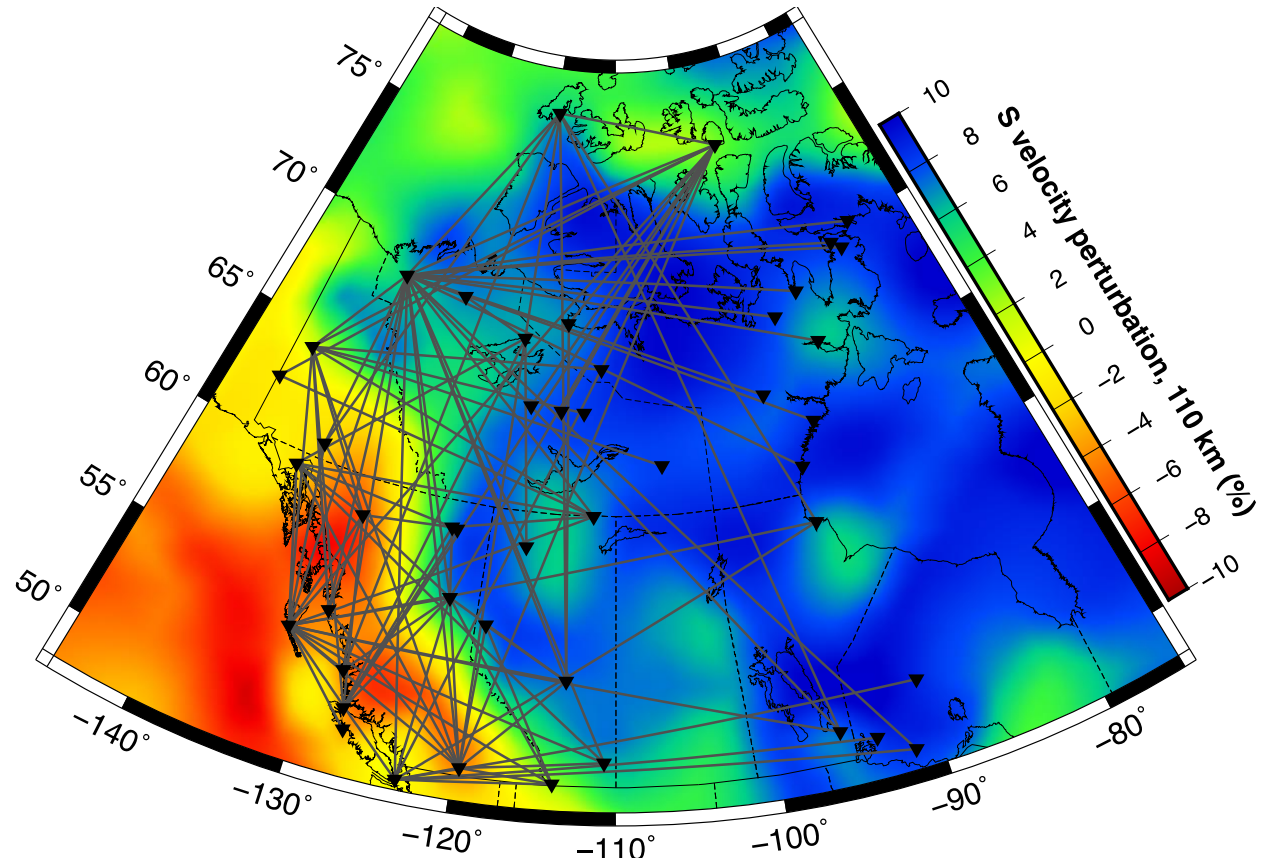
- 404 North, R.G., and Basham, P.W. 1993. Modernization of the Canadian National Seismograph  
405 Network. *Seismological Research Letters* **64**: 41. *Seis. Res. Let.*
- 406 Parker, R.L. 1994. *Geophysical Inverse Theory*. Princeton University Press.
- 407 Ren, Y., Stutzmann, E., van der Hilst, R., and Besse, J. 2007. Understanding seismic  
408 heterogeneities in the lower mantle beneath the Americas from seismic tomography and  
409 plate tectonic history. *J. Geophys. Res.* **112**: 302.
- 410 Sato, Y. 1955. Analysis of Dispersed Surface Waves by means of Fourier Transform I. *Bull.*  
411 *Earthquake Res. Tokyo Univ.* **33**: 33–47.
- 412 Schaeffer, A., and Lebedev, S. 2014. Imaging the North American continent using waveform  
413 inversion of global and USArray data. *Earth and Planetary Science Letters* **402(C)**: 26–41.  
414 Elsevier B.V. doi:10.1016/j.epsl.2014.05.014.
- 415 Schaeffer, A.J., Audet, P., Mallyon, D., Currie, C.A., and Gu, Y.J. 2017. Transient tectonic  
416 transition from Canadian Cordillera to stable shield?  
417 . pp. 1–1.
- 418 Stein, S., and Wysession, M. 2003. *An Introduction to Seismology, Earthquakes, and Earth*  
419 *Structure*. John Wiley & Sons.
- 420 Thorkelson, D.J., and Taylor, R.P. 1989. Cordilleran slab windows. *Geol* **17(9)**: 833–836.  
421 GeoScienceWorld. doi:10.1130/0091-7613(1989)017<0833:CSW>2.3.CO;2.
- 422 Tian, Y., and Zhao, D. 2012. P-wave tomography of the western United States: Insight into the  
423 Yellowstone hotspot and the Juan de Fuca slab. *Physics of the Earth and Planetary Interiors*  
424 **200-201**: 72–84. Elsevier. doi:10.1016/j.pepi.2012.04.004.
- 425 van der Lee, S., and Frederiksen, A. 2005. Surface wave tomography applied to the north  
426 american upper mantle. *Geophysical monograph*.
- 427 van der Lee, S., and Nolet, G. 1997a. Upper mantle S velocity structure of North America. *J.*  
428 *Geophys. Res.* **102(B10)**: 22815–22838.
- 429 van der Lee, S., and Nolet, G. 1997b. Seismic image of the subducted trailing fragments of the  
430 Farallon plate. *386(6622)*: 266–269.
- 431 Whitmeyer, S., and Karlstrom, K. 2007. Tectonic model for the Proterozoic growth of North  
432 America. *Geosphere* **3(4)**: 220.
- 433 Yuan, H., French, S., Cupillard, P., and Romanowicz, B. 2014. Lithospheric expression of  
434 geological units in central and eastern North America from full waveform tomography. *Earth*  
435 *and Planetary Science Letters* **402(C)**: 176–186. Elsevier B.V.  
436 doi:10.1016/j.epsl.2013.11.057.
- 437

Zaporozan *et al.*, *Surface-Wave Images of Western Canada, draft for resubmission*438 **Figures**

439

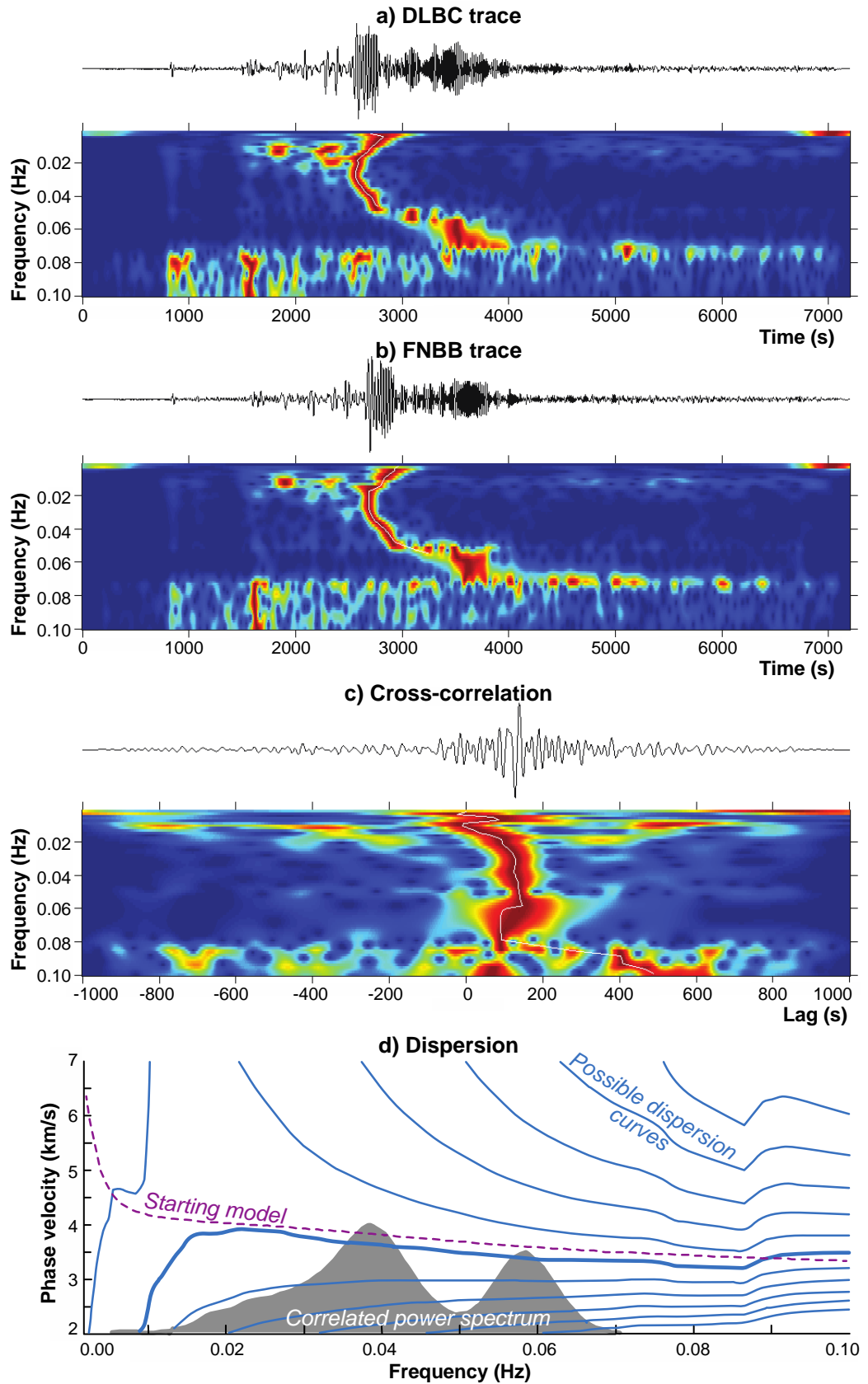
440 Figure 1: Seismic stations used in this study (red triangles), overlain on topography. Black lines  
441 indicate major tectonic boundaries (simplified from Whitmeyer and Karlstrom, 2007). Map  
442 projection: Lambert conic centred at 63°N, 110°W with standard parallels at 53°N and 73°N; the  
443 same projection is used for all other maps in this paper.

## Zaporozan et al., Surface-Wave Images of Western Canada, draft for resubmission



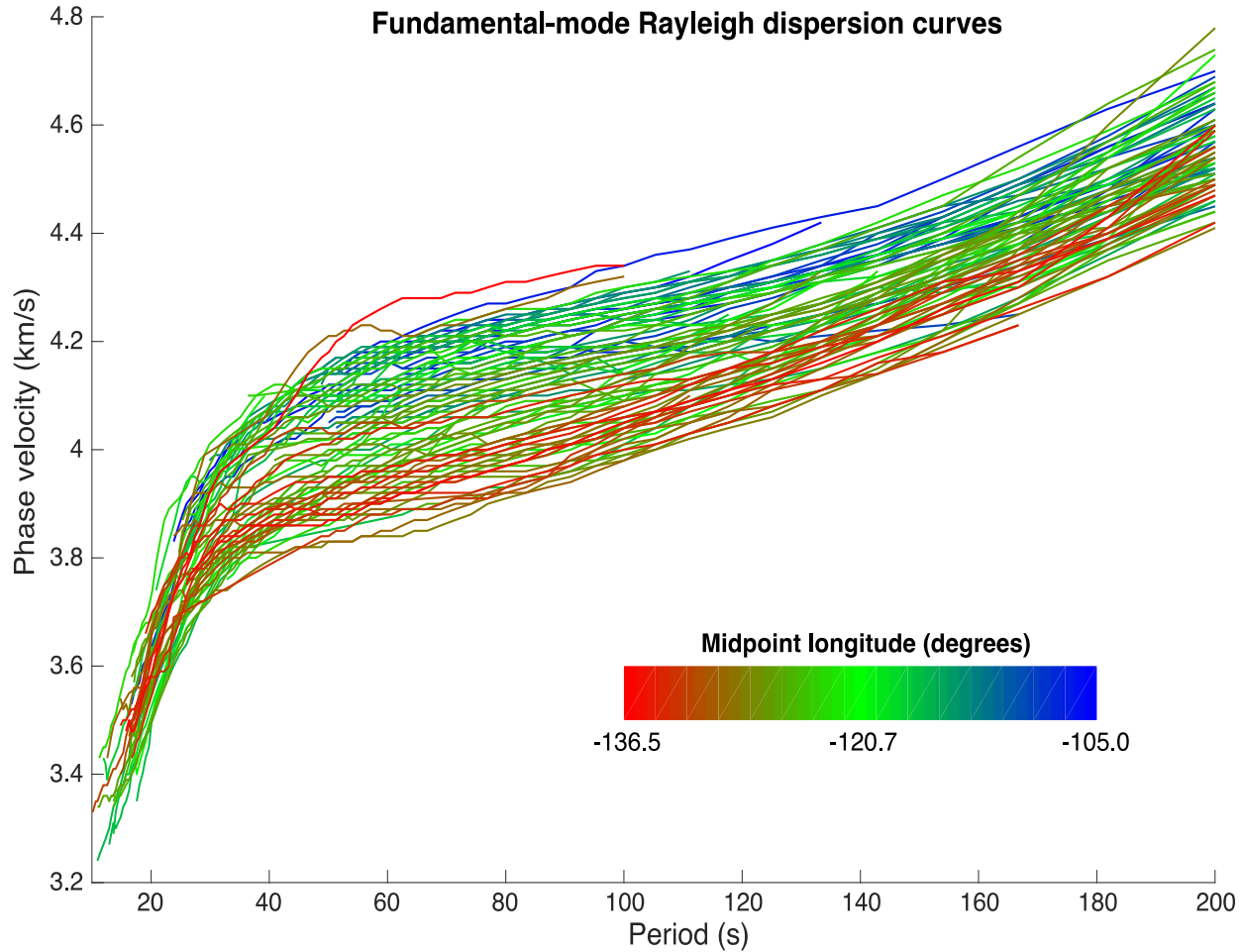
444

445 Figure 2: Two-station paths (grey lines) analyzed in this study. Background is seismic  $S$  velocity  
446 at 110 km depth, from the tomographic model of Schaeffer and Lebedev (2014).

Zaporozan et al., *Surface-Wave Images of Western Canada, draft for resubmission*

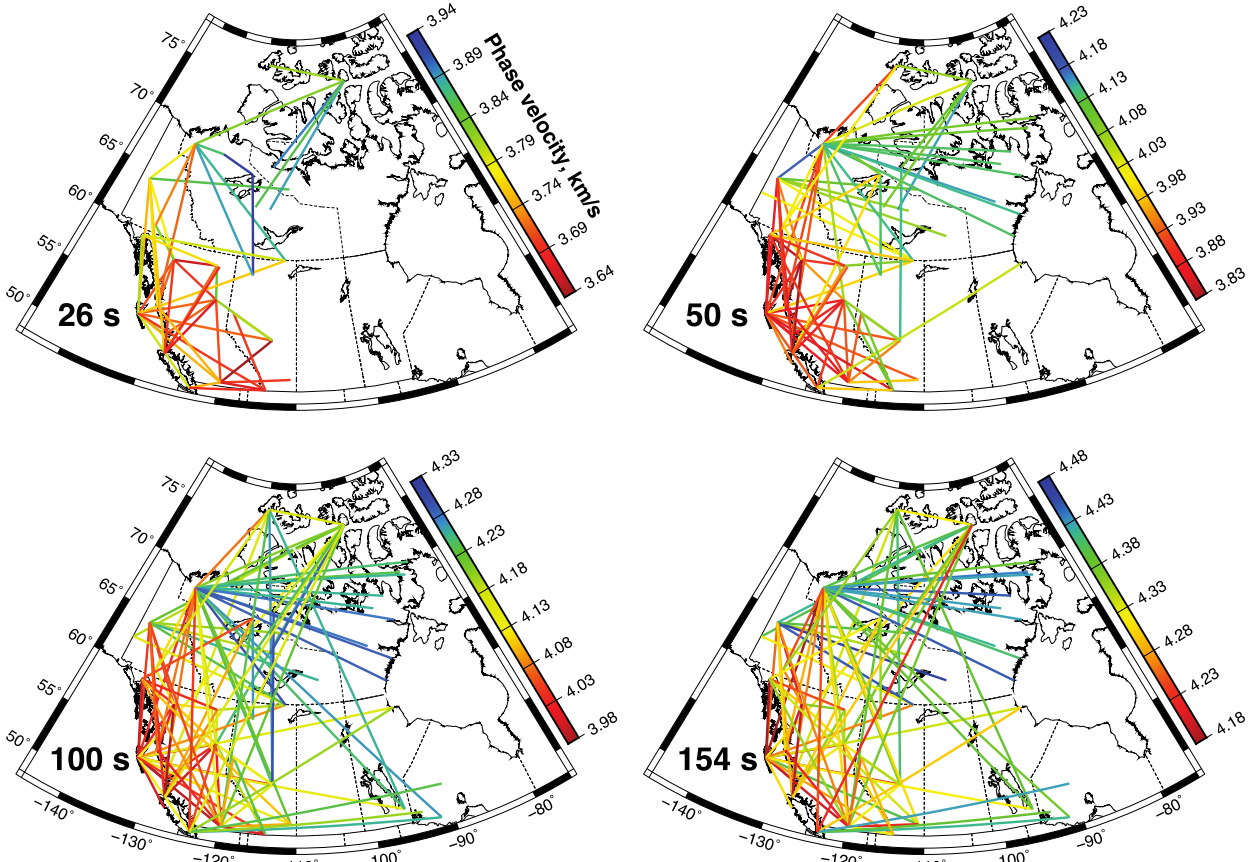
## Zaporozan et al., Surface-Wave Images of Western Canada, draft for resubmission

448 Figure 3: Two-station analysis for an event recorded at DLBC (Dees Lake, British Columbia)  
 449 and FNBB (Fort Nelson, British Columbia). Individual traces (a, b) are shown along with a time-  
 450 frequency analysis; the thin white line indicates group arrival time. The two traces are cross-  
 451 correlated (c) and the cross-correlation phase determines possible Rayleigh phase-velocity curves  
 452 (d, blue lines). Due to the  $2n\pi$ -radian ambiguity of phase, curves are closely spaced at high  
 453 frequencies; at lower frequencies, only one is plausible (thick line) and may be followed to  
 454 higher frequency. Here, the curve is usable from  $\approx 0.02$  to  $0.07$  Hz.



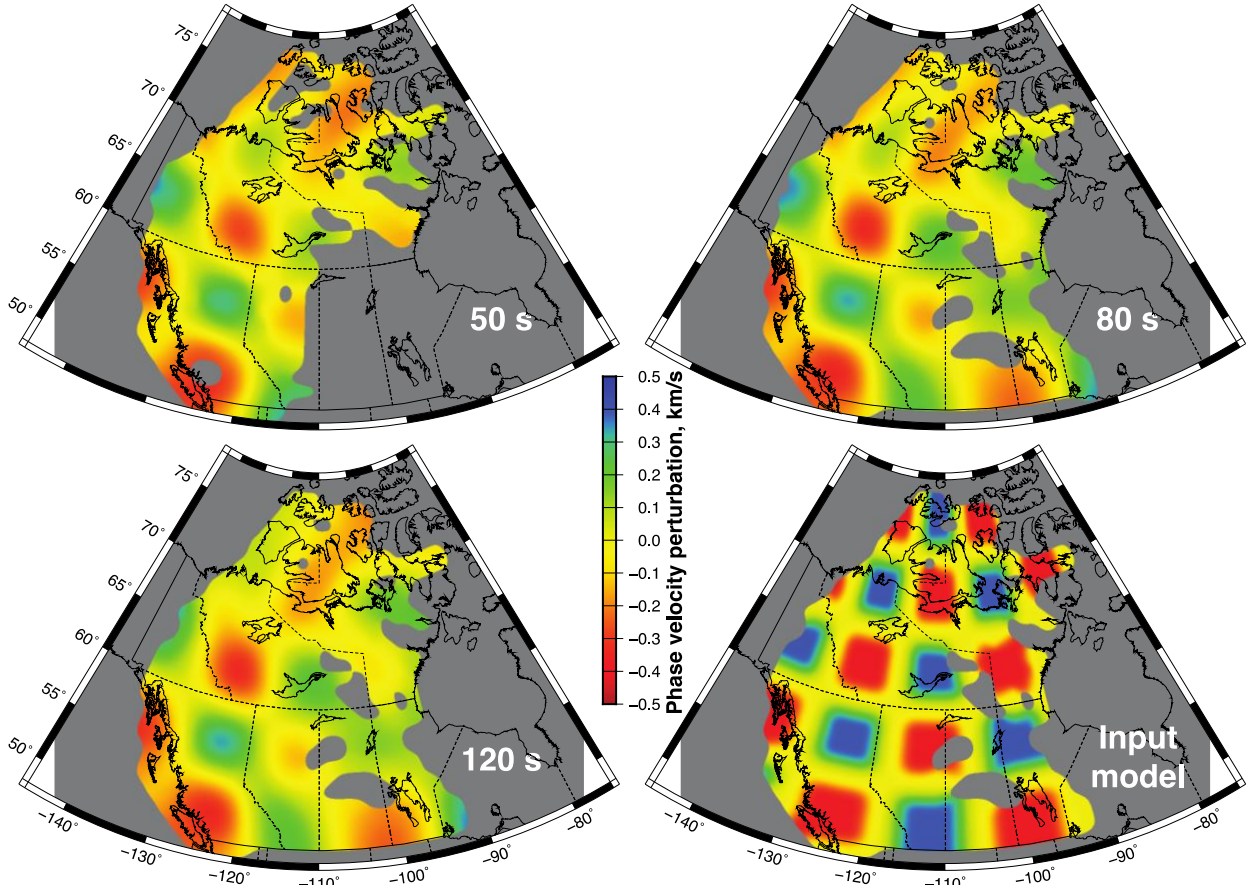
455  
 456 Figure 4: Average phase-velocity dispersion curves for all paths examined in this study. The  
 457 curves are coloured based on the midpoint longitudes of the corresponding two-station paths.

## Zaporozan et al., Surface-Wave Images of Western Canada, draft for resubmission



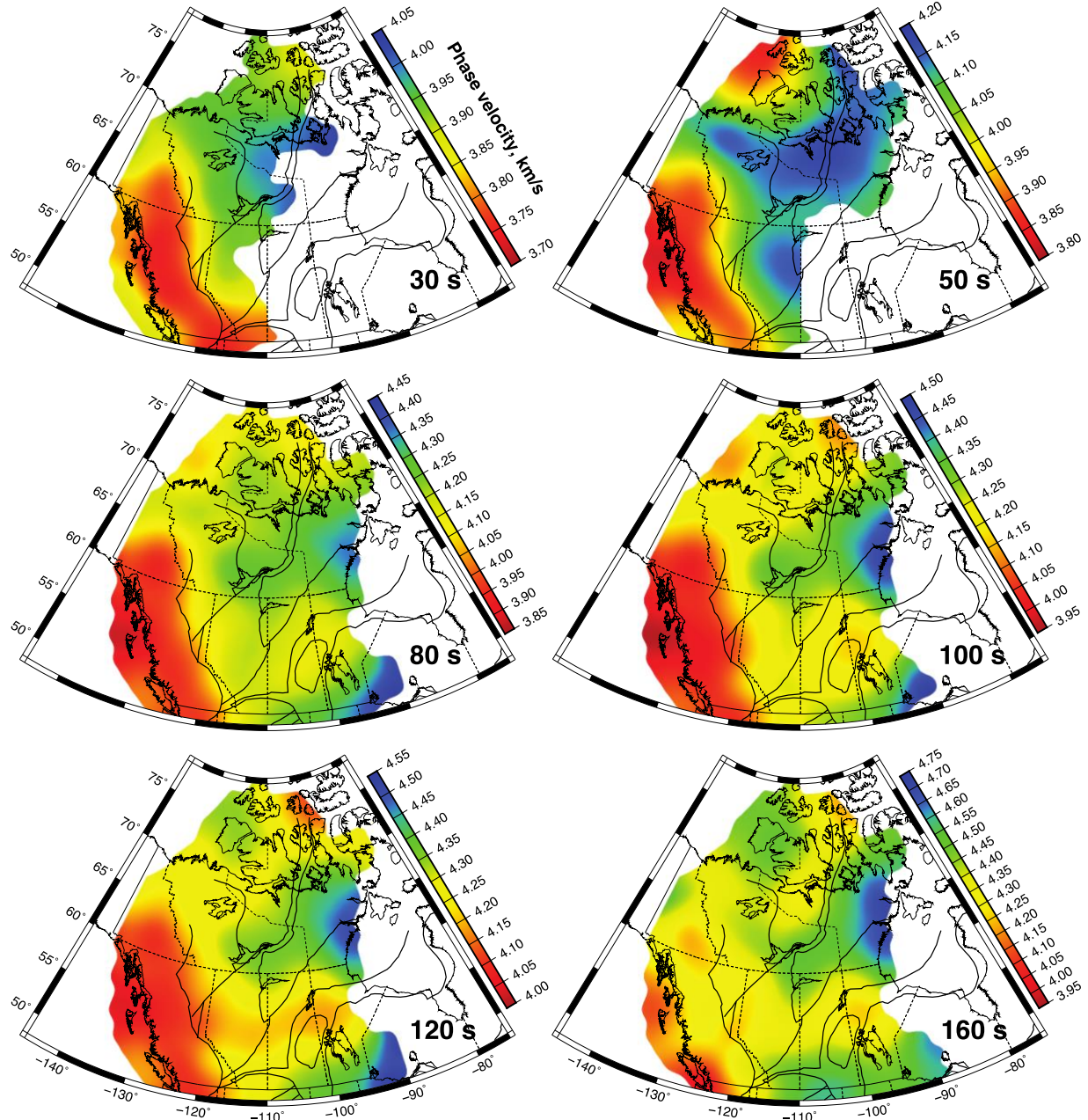
458

459 Figure 5: Phase velocities at four representative periods, plotted as shaded lines along the  
460 corresponding two-station great-circle paths. Note that the colour scale differs between panels.

Zaporozan et al., *Surface-Wave Images of Western Canada, draft for resubmission*

461

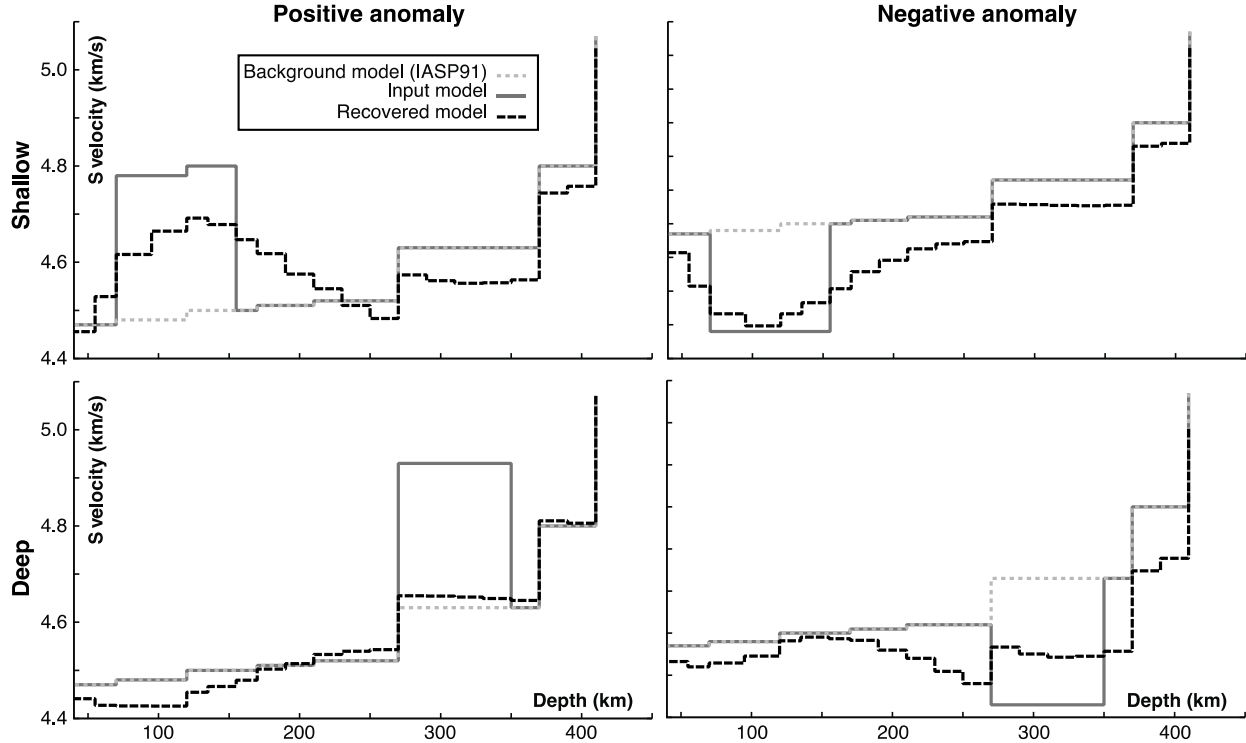
462 Figure 6: Checkerboard resolution tests for phase-velocity tomography, at three representative  
463 periods. Greyed-out model cells were not sampled by rays. The colour scale is the same for all  
464 plots.

Zaporozan et al., *Surface-Wave Images of Western Canada, draft for resubmission*

465

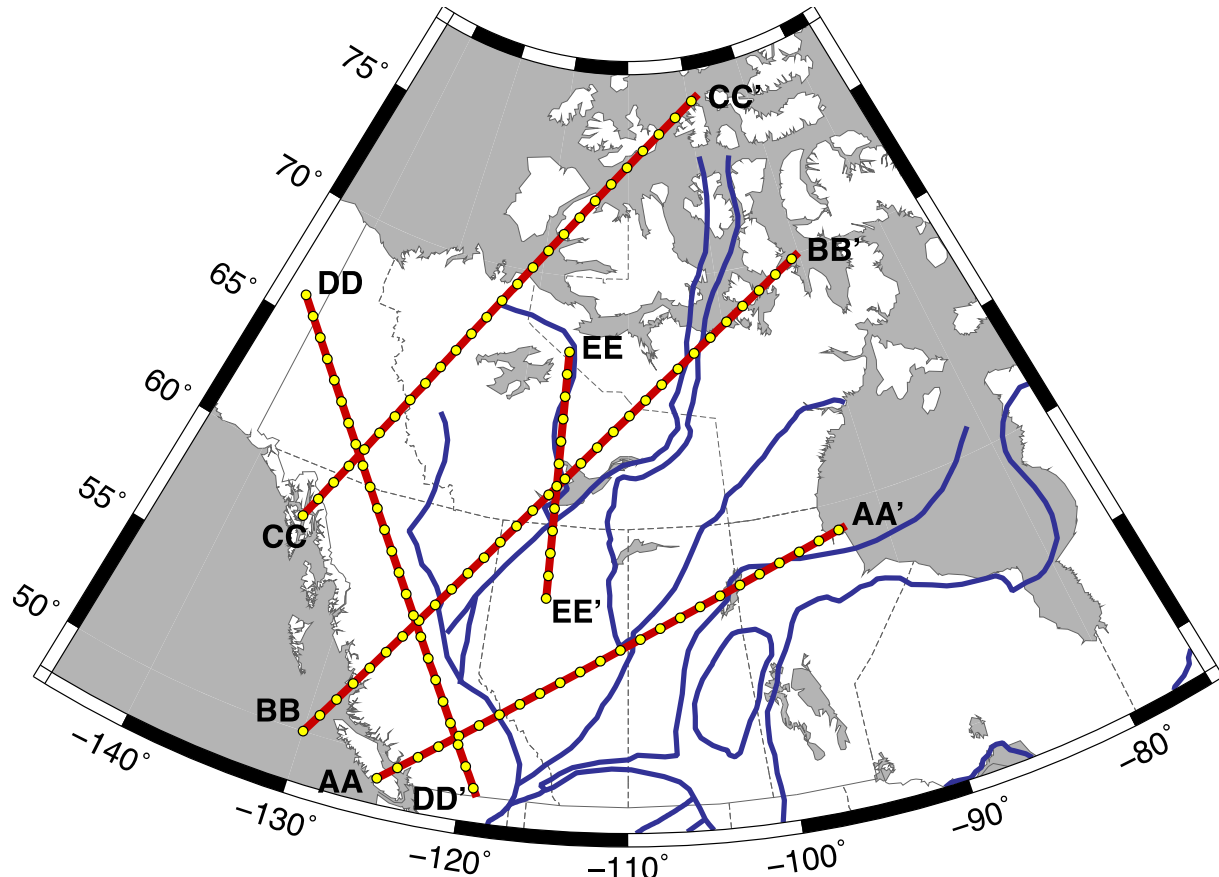
466 Figure 7: Recovered Rayleigh phase-velocity maps at six periods. The colour scale varies  
467 between plots. Black lines are tectonic boundaries from Figure 1.

## Zaporozan et al., Surface-Wave Images of Western Canada, draft for resubmission



468  
469 Figure 8: Synthetic tests of depth resolution. The input model (solid grey) contains a perturbation  
470 from the background (grey dotted); the recovered model (black dashed) is the result of  
471 generating synthetic data from the input model, then inverting the result.

Zaporozan et al., *Surface-Wave Images of Western Canada, draft for resubmission*

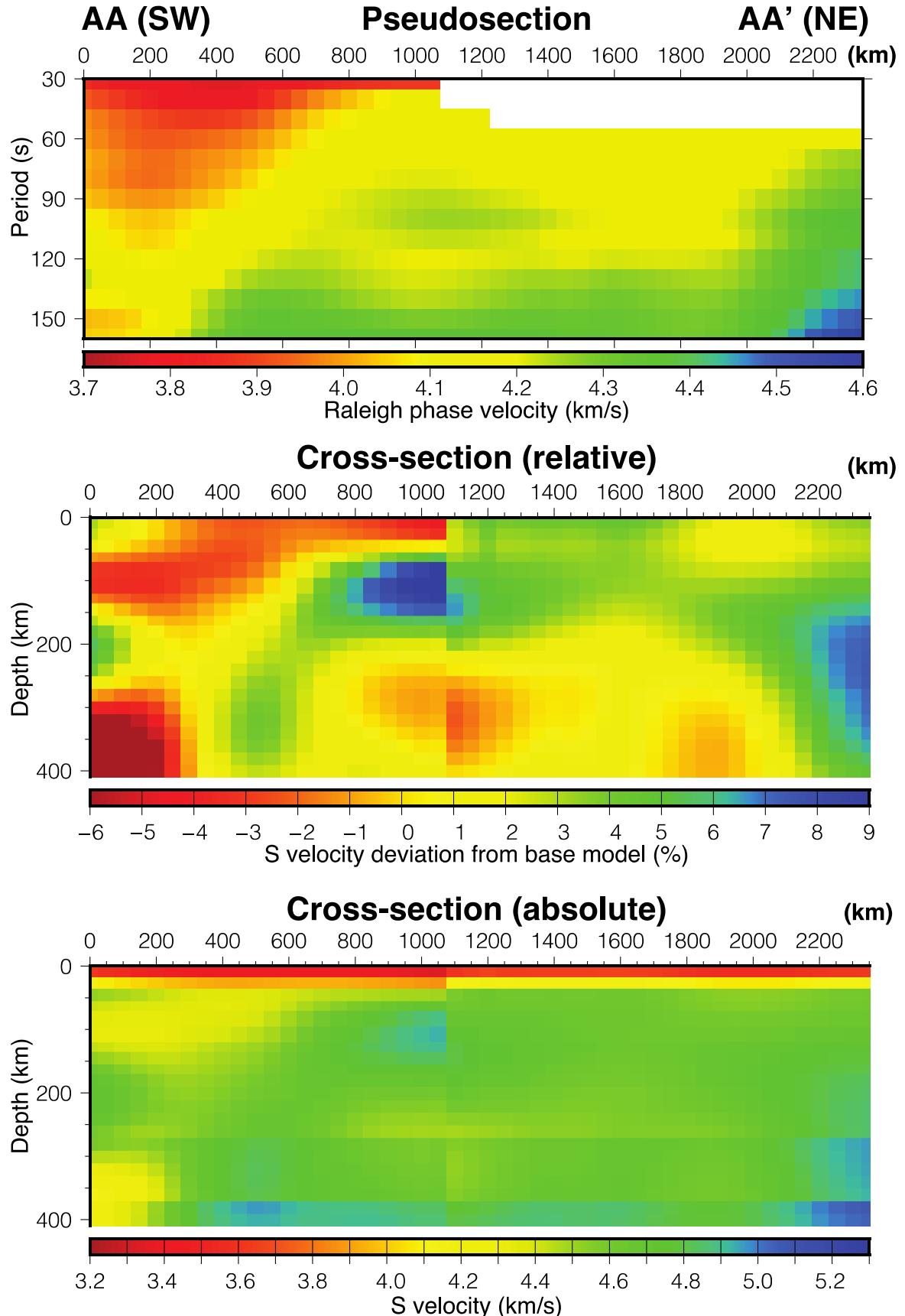


472

473 Figure 9: Locations of transects (red lines) inverted to form cross-sections. Yellow dots mark

474 100 km intervals. The blue lines are tectonic boundaries from Figure 1.

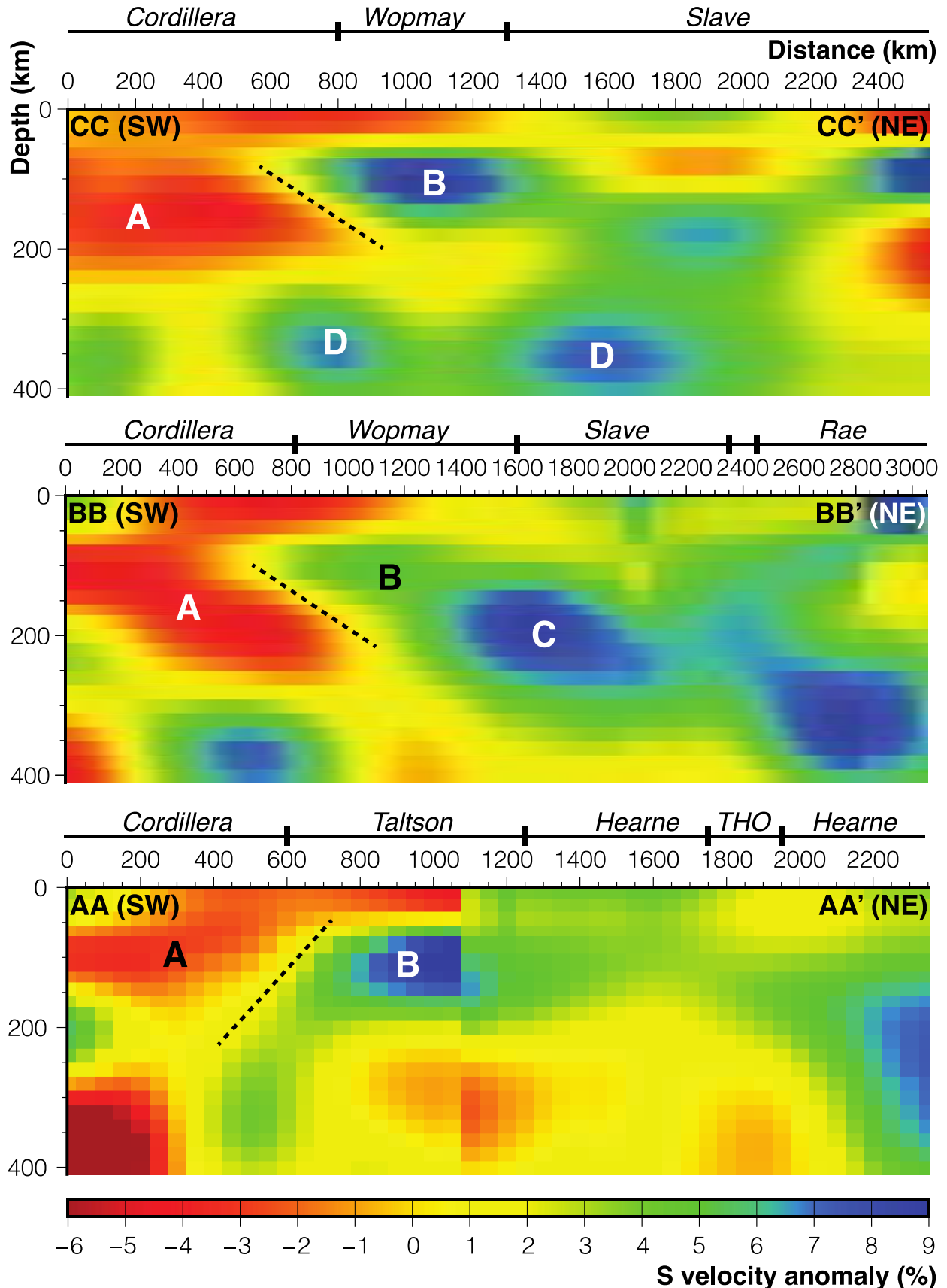
Zaporozan et al., Surface-Wave Images of Western Canada, draft for resubmission



*Zaporozan et al., Surface-Wave Images of Western Canada, draft for resubmission*

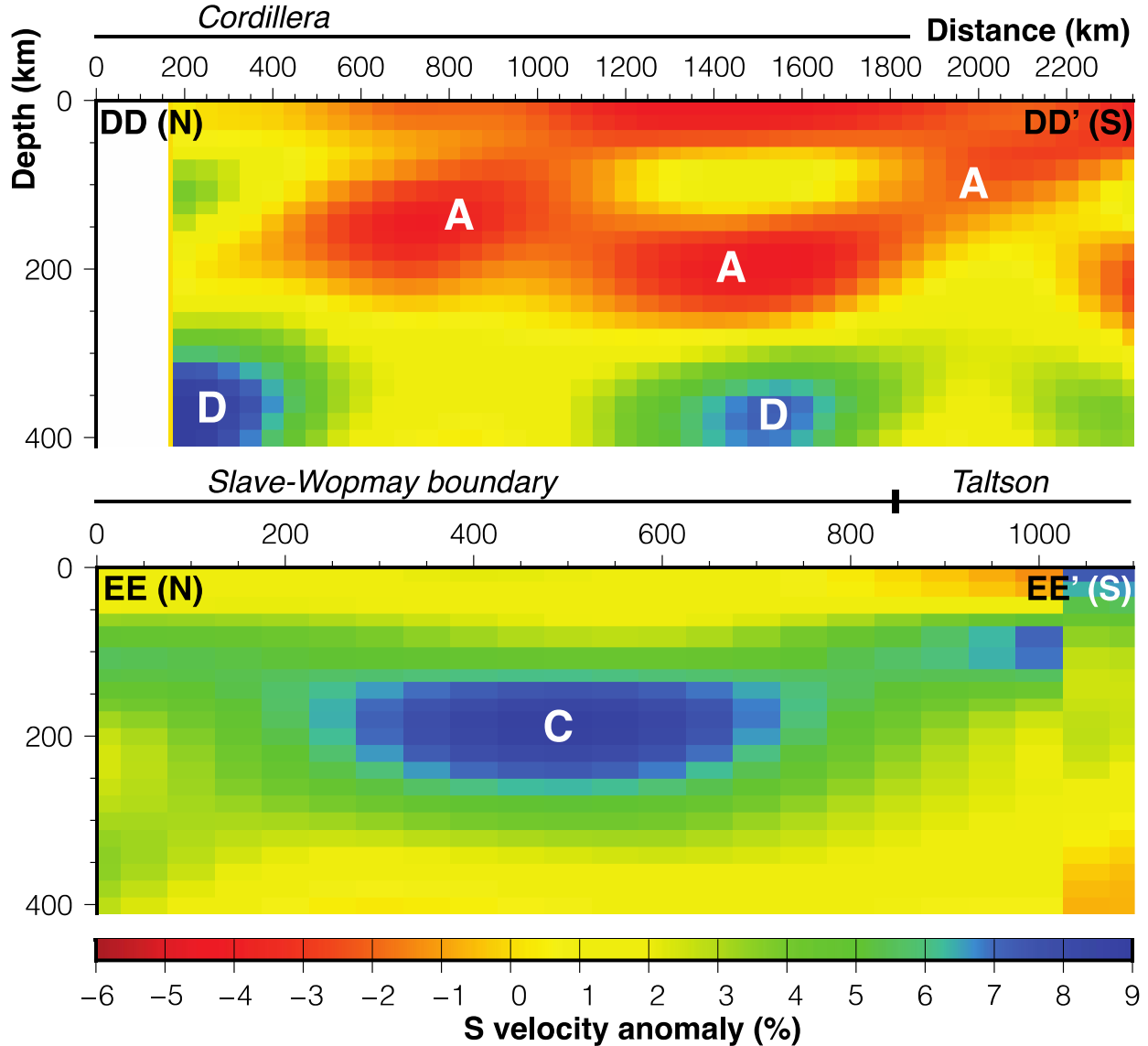
476    Figure 10: Example of the cross-section generation process for transect AA-AA'. A  
477    pseudosection (top) is extracted from dispersion maps, then each column is inverted separately to  
478    form a 1-D model. Concatenation of these 1-D models generates a cross-section, presented in  
479    terms of relative (middle) or absolute (bottom) velocity; the base model is IASP91.

## Zaporozan et al., Surface-Wave Images of Western Canada, draft for resubmission



Zaporozan *et al.*, Surface-Wave Images of Western Canada, draft for resubmission

481 Figure 11: Three relative-velocity cross-sections perpendicular to the Cordillera-craton  
 482 boundary, ordered from north to south. Labels at the top of each indicate the tectonic provinces  
 483 sampled. Letters indicate features discussed in text; dashed line indicates approximate 0%  
 484 contour between features A and B.



485  
 486 Figure 12: Additional relative-velocity cross-sections along the strike of the Cordillera (top) and  
 487 across a high-velocity feature (C) near Great Slave Lake.